THE ASTROPHYSICAL JOURNAL, 191:331–348, 1974 July 15

CHARGE COMPOSITION AND ENERGY SPECTRA OF COSMIC-RAY NUCLEI AT ENERGIES ABOVE 20 GeV PER NUCLEON*†

EINAR JÚLIUSSON
Enrico Fermi Institute and Department of Physics, Laboratory for Astrophysics and Space Research, University of Chicago
Received 1973 November 30; revised 1974 January 21

ABSTRACT

An instrument to measure the charge composition and energy spectra of cosmic-ray nuclei of charge $Z = 3$ and above has been exposed for a net total of 7.6 m^2 sr hours in three balloon flights during 1971 and 1972. The instrument is a scintillation-Cerenkov counter telescope, including two gas Cerenkov counters for energy measurements above 20 GeV per nucleon, and up to about 100 GeV per nucleon. In this paper we present the charge composition and energy spectra that have been measured in that energy range. The nuclear composition has been found to change with energy. The flux of nuclei produced by spallation of source nuclei in the Galaxy has been found to decrease faster with increasing energy than the flux of source nuclei. The carbon to oxygen ratio measured above 20 GeV is significantly lower than measured at low energy. Iron exhibits a flatter energy spectrum than other nuclei. The results are interpreted as showing that the high-energy nuclei have traversed less material than the low-energy nuclei.

Subject heading: cosmic rays

I. INTRODUCTION

Measurements of the charge and energy composition of cosmic-ray nuclei made over the past decade have revealed much information about the origin and propagation of the cosmic radiation. The fact that these measurements did not indicate a change in the nuclear composition over a wide energy range has been interpreted to show (1) an energy-independent source composition or charge-independent acceleration mechanism; (2) an energy-independent propagation of the nuclei in the Galaxy. This last requirement is necessary since some of the nuclei we observe here at Earth are *secondary*, i.e., have not originated in the same sources as the *primary* nuclei but are produced by spallation of the primary or source nuclei, interacting with interstellar matter in the Galaxy. The result that these secondary nuclei have the same energy spectra as the source nuclei indicates that the energy spectra of the cosmic rays are not noticeably modified by the propagation through interstellar space. The spectra measured at Earth have therefore been assumed to be the same as the source spectra. In models describing the propagation and spallation of the nuclei in the Galaxy, energy-independent spallation cross-sections and amount of matter traversed, diffusion coefficients, and confinement times have been postulated (Shapiro and Silberberg 1970). These considerations apply to energies above a few GeV per nucleon. At lower energies it is known that this picture cannot be true, since energy dependence of the spallation cross-sections, energy losses, and effects of the solar modulation enter the picture. The fact that differences in the nuclear composition have not been found even in this energy range has been interpreted as showing a significant energy loss (adiabatic deceleration) in the solar system so that the low energies measured at Earth correspond to significantly higher energies in nearby interstellar space.

While no clear energy dependence of the composition has been found and agreed upon by earlier observations, individual measurements did not always agree with each other. Variations in composition with energy have been reported, but these variations have later not been confirmed. This picture of energy-independent composition could thus change with measurements of better charge and energy resolution and improved statistical and systematic accuracy. Also, measurements have usually been limited to energies below a few GeV per nucleon. This is due to both the rapidly decreasing fluxes with energy and the technical difficulties encountered in measuring the high energies.

It is the purpose of this experiment to measure the charge composition and energy spectra of the cosmic-ray nuclei at higher energies and with better statistics and resolution than has previously been obtained. Special emphasis has been put on the energy range above 20 GeV per nucleon. In this paper we present the completed analysis of our measurements of the cosmic-ray charge composition and energy spectra above 20 GeV per nucleon, obtained in three balloon flights in 1971 and 1972. Our initial results have already been published (Júliusson, Meyer, and Müller 1972; Júliusson and Meyer 1973) and reported in conferences (Júliusson 1973; Júliusson *et al.* 1973). An analysis of the data at lower energies will be published later. We have found that the composition at high energies differs in many ways from the composition measured at low energies. Similar differences have also been

* This work was supported in part by the National Aeronautics and Space Administration under grant NGL 14-001-005.

† Submitted to the Department of Physics, University of Chicago, Chicago, Illinois, in partial fulfillment of the requirements for the Ph.D. degree.

reported by other observers, using for the energy determination quite different techniques like magnetic spectrometer (Smith *et al.* 1973), Cerenkov counters and the geomagnetic field (Webber *et al.* 1973*a*, *b*), and ionization spectrometer (Ormes and Balasubrahmanyan 1973; Ormes, Balasubrahmanyan, and Arens 1973; Balasubrahmanyan and Ormes 1973). These new findings are important for an understanding of the origin of cosmic rays and their propagation in interstellar space.

II. INSTRUMENT AND FLIGHTS

The instrument used for our measurements is shown schematically in figure 1. The basic telescope consists of three plastic counters C1, C3, C4. Two of these counters, C1 and C4, are Cerenkov counters made from Pilot 425 in thicknesses of 10 and 5 mm, while the third one, C3, is a scintillation counter made from Pilot Y and 5 mm in thickness. These counters measure the charge and energy of each nucleus passing through the instrument over the energy range 0.33 GeV per nucleon to a few GeV per nucleon. To obtain maximum uniformity of the counters they are housed in light-integration boxes lined with high-reflectance (~97 percent) white material. We estimate the uniformity of the counters to be better than 1 percent. For the width, or relative width, of distributions we shall always use standard deviation σ, or σ/mean. To improve the path length distribution in C1 and thereby the charge resolution of the instrument, that counter has been segmented into six parts. Each segment is perpendicular to the line connecting the center of that segment to the center of C3. The segmentation improves the σ/mean of the path length distribution in C1 from 5 to 2 percent, which allows good charge separation up to the charge of iron. The instrument was flown once in this version I. The geometric factor for version I as determined by the C1 · C3 coincidence is 850 cm² sr.

A change in the counter configuration was made after the first flight. In this version II the counters C1 and C4 are scintillation counters (Pilot Y) of 11-mm thickness, while C3 is a Cerenkov counter (Pilot 425) of 22-mm thickness. The change was made to improve the low-energy (E less than a few GeV per nucleon) resolution and does not much affect the high-energy data presented here. In version II the geometric factor of the instrument is 950 cm² sr, as determined by the C1 · C4 · $\bar{G}$ coincidence. We will hereafter, unless otherwise specified, refer to version II of the instrument.

The instrument contains two gas Cerenkov counters for energy measurements above 20 GeV per nucleon. These measurements use the dependence of the Cerenkov light output L on the energy of the nucleus which can be written

$$L \propto (1 - 1/n^2\beta^2) \propto (1 - P_0^2/P^2) . \qquad (1)$$

Here n is the index of refraction of the Cerenkov material, β is the velocity of the nucleus, P is the momentum per nucleon of the nucleus. Below the *threshold momentum* P_0 the light output will be zero. The upper gas counter C2A utilizes the light integration method to collect the light while the lower one C2B uses mirrors to focus the Cerenkov light into the phototubes. These two types of counters complement each other since the focusing counter C2B is rather insensitive to noise and scintillations in the gas, while the white counter C2A has good resolution, limited only by photoelectron statistics. The energy range that can be covered depends on the type and pressure of the gas in the counters. To obtain a higher index of refraction we have used freon-12 in all flights. It was used in C2A in version I and in C2B for the two flights of version II. Filled with this gas at atmospheric pressure, the counter has a threshold energy E_0 of 19 GeV per nucleon which then corresponds to the lowest energy we can measure with the gas counters. To provide the lower index of refraction we used air in flight 1, CO_2 in flight 2, and an SF_6 + methane mixture in flight 3, leading to threshold energies of 40, 31, and 24 GeV per nucleon in flights 1, 2, and 3, respectively. If the pulse-height resolution of the counter is limited by photoelectron statistics, the *maximum resolvable energy*, $E_{\rm int}^{\rm max}$, the energy that corresponds to a signal 1 σ below maximum signal, is seen from

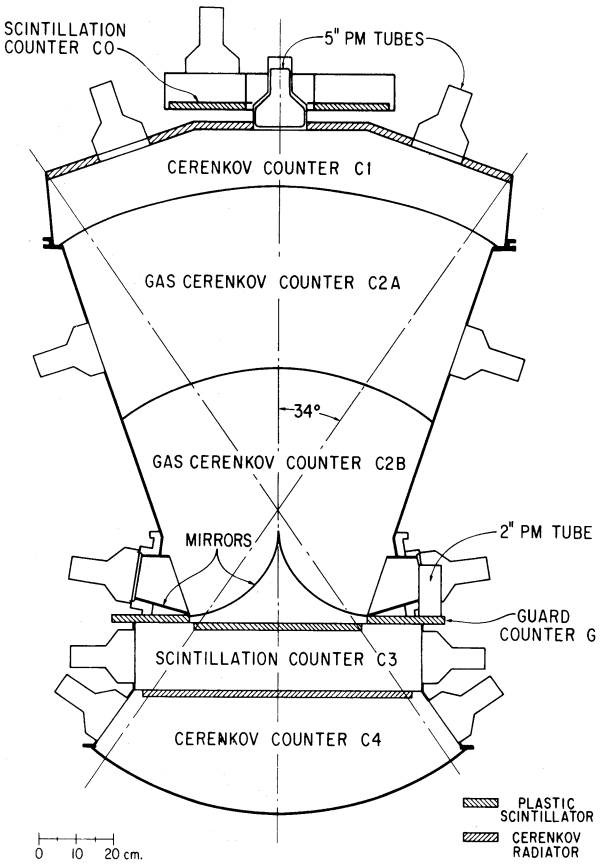

FIG. 1.—A schematic cross-section of the High Energy Nuclei telescope (HEN).

equation (1) to be

$$E_{\rm int}^{\rm max} = E_0 \times N_{\rm pe}^{0.25}, \quad (2)$$

where $N_{\rm pe}$ is the number of photoelectrons for a nucleus traveling with velocity c, and where we have used the approximation $E = P$. The value $E_{\rm int}^{\rm max}$ is roughly the maximum energy above which the composition can be measured. Measurements of the composition above the energy $E_{\rm int}$ correspond to measurements at the energy $E_{\rm diff}$. Assuming that all nuclei have power-law spectra with a spectral index close to γ, the connection between the two energies is

$$E_{\rm diff} = e^{1/(\gamma-1)} E_{\rm int}\,. \quad (3)$$

Using CO_2 in the C2A counter we obtain approximately 50 photoelectrons for a relativistic oxygen nucleus. While $N_{\rm pe}$, and thus the maximum energy, depends on the charge measured, we can for most charges cover the energy range 20–100 GeV per nucleon in each flight.

The instrument contains a guard counter G that helps to eliminate nonnuclear background, and a small counter C0 can be used to limit the opening angle of the telescope. A more detailed description of the instrument will be published elsewhere.

The first flight of the instrument was carried out from Palestine, Texas, in the fall of 1971. It floated at a rather constant altitude under 4.8 g cm^{-2} vertical depth of residual atmosphere for 30 hours. The geomagnetic cutoff ranged from about 4.6 to 5.6 GV during the flight. Two additional flights were made from Cape Girardeau in the fall of 1972. Both flights were terminated after 35 hours at an average residual atmosphere of 5.8 g cm^{-2} but varying from 4 to 12 g cm^{-2} during these flights. The geomagnetic cutoff varied from 2.5 to 2.0 GV during the flights. These three flights of the instrument thus resulted in 100 hours of exposure at altitude. The net collection factor obtained is 7.6 m^2 sr hours.

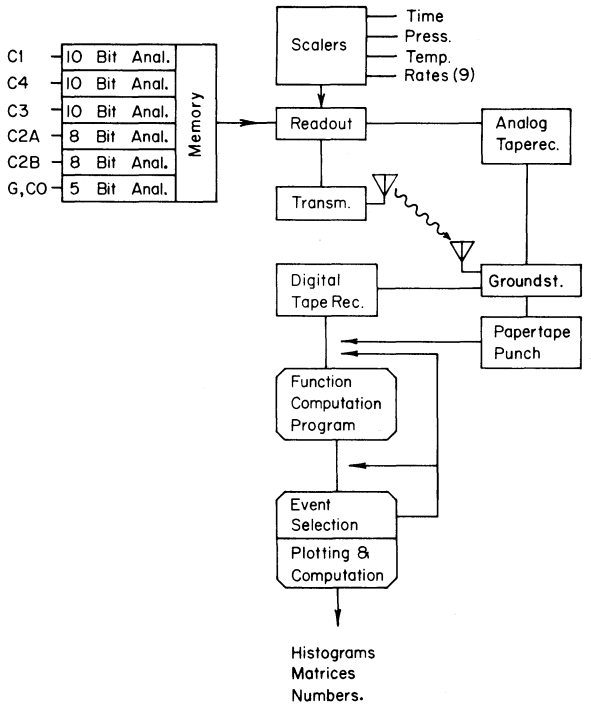

FIG. 2.—A schematic diagram of the data flow through the instrument, ground equipment, and analysis programs.

III. DATA ANALYSIS

The data flow through the instrument, ground equipment, and the two analysis programs is shown schematically in figure 2. The programs compute additional information or functions for each event, select events based on the values taken by any of the functions, and plot out histograms and matrices of the functions.

a) Event Selection and Corrections

The event selection is the cornerstone of the analysis. We set up criteria to select, for example, all noninteracting nuclei of charge Z in an energy range ΔE. Such a selection can evidently not be perfect, but we assume that the true number of nuclei of charge Z in the energy range ΔE can be obtained by adding a (small) correction to the measured number, i.e., the number satisfying the selection criteria. Alternatively the measured number should be multiplied by a correction factor to obtain the true number.

Such a correction is twofold. First, events that belong to a particular interval may not all pass the selection criteria, and a positive correction must be added to the measured number. Second, unrelated events may not all be rejected by the selection criteria and a negative correction must be added to the measured number. These two corrections, which shall be called the *selection correction* and the *background correction*, respectively, apply to the primary selection of noninteracting nuclei. When an event that fails the selection criteria is not discarded but rather falls (incorrectly) into the neighboring charge or energy interval, the correction, positive or negative, that must be applied shall be called the *overlap correction*. This correction will be discussed in greater detail in § III*b* and in the Appendix.

To exemplify how noninteracting nuclei are selected from the raw data we show in figure 3 a matrix of the pulse height in C1 versus the pulse height in C4. Besides the selection done by the instrument, namely that C1 and C4 each are above a certain threshold, and also that events very low in C1 and C4 (lithium only) are required to trigger C3 above a very low threshold, the selection criterion G = 0, i.e., no signal in the guard counter, has been applied. The figure shows data collected in 1 hour of flight 2. It shows the noninteracting nuclei that we wish to select as well as the interacting nuclei and unrelated background events. These events include nonnuclear background, nuclei outside the acceptance cone of the instrument, and low-energy α-particles.

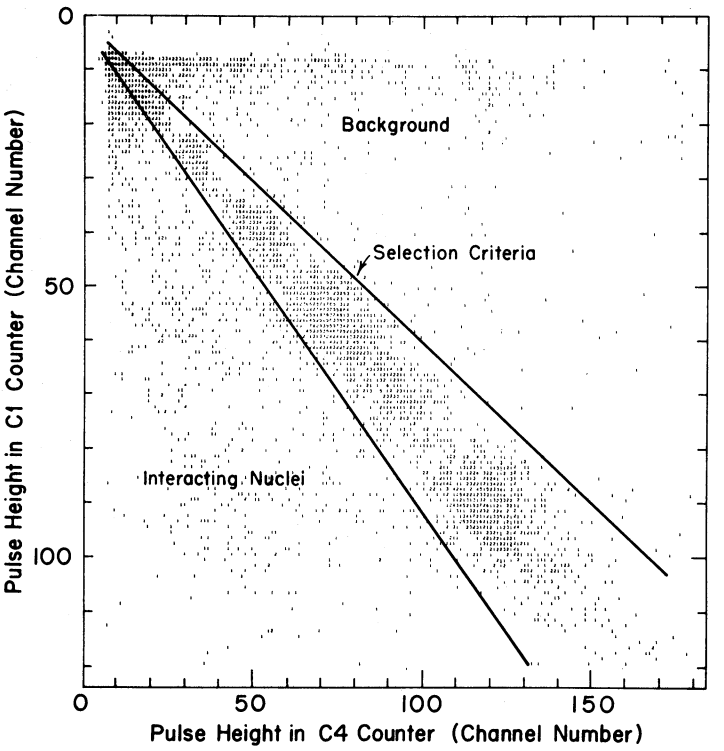

FIG. 3.—Matrix of pulse height in C1 counter versus pulse height in C4 counter obtained in 1 hour of flight 2. Selection criteria used for the analysis, accept only data between the two lines.

To select noninteracting nuclei we ask for an agreement between the two identical counters C1 and C4, requiring $0.8 < C1/C4 < 1.2$. C1 and C4 are the pulse heights of counters C1 and C4, normalized such that the mean of C1/C4 is 1.0 for accepted events. These selection criteria are shown as lines in figure 3. To separate the charge and energy dependence of the signal we then plot the Cerenkov counter versus the average of the two scintillation counters. This is shown in figure 4 which contains again 1 hour of data from flight 2. The figure shows a matrix of Z3 versus an average of Z1 and Z4, after application of the C1/C4 and the guard counter selection criteria. Z1, Z3, Z4 are functions computed by the first analysis program. Z1 is basically the square root of C1. It involves the following: (1) C1 is randomized to eliminate the channel structure, i.e., channel 20 becomes some random number between 19.5 and 20.5; (2) C1 is normalized, and linearized to correct for the non-linearity of the Pilot Y light output (see fig. 6), and a small electronic zero offset is corrected; (3) C1 is corrected for small drifts during the flight. Since the drift is less than 1 percent, the improvement of the data by including this correction is very small.

The figure shows a clear charge separation with no overlap between adjacent charges and little or no background. The corrections needed on the data shown in figure 4 are small. The background correction can be mostly ignored but a small selection correction must be applied. We have to correct for the selection made by the instrument which eliminates in this flight 2 only a very small fraction of the low-energy lithium. The guard counter criterion used in figure 3 ($G = 0$) eliminates little carbon and lighter nuclei but a larger fraction of heavier nuclei and almost all nuclei above silicon, due to δ-rays that traverse the guard counter. Consequently, a different selection criterion is used for this analysis and for obtaining figure 4. The maximum guard-counter signal allowed is 8 percent of what it would be if the nucleus had passed through the guard counter. This criterion eliminates about 2 percent of the noninteracting nuclei and close to the same fraction for all charges. The last criteria, the limits on C1/C4, are charge sensitive and, as seen on figure 3, eliminate only a very small fraction of carbon and heavier nuclei, but a somewhat larger fraction of the lighter nuclei, due to the wider Landau distribution of their signal in C1 and C4.

While the background correction is sufficiently small to be ignored for the *low-energy* data shown in figure 4, this is not the case for our *high-energy* data, that is, in the energy range covered by only one of the gas counters. We shall in this paper define high energy as $E > 20$ GeV per nucleon and low energy as $E < 20$ GeV per nucleon. In figure 5 is shown a scintillator-Cerenkov matrix for nuclei triggering C2B. The signal required in C2B is 10 percent of the maximum signal, i.e., the signal from a nucleus traveling with velocity c. These are data from flights 2 and 3 combined. Comparing figure 4 with figure 5 we see two types of

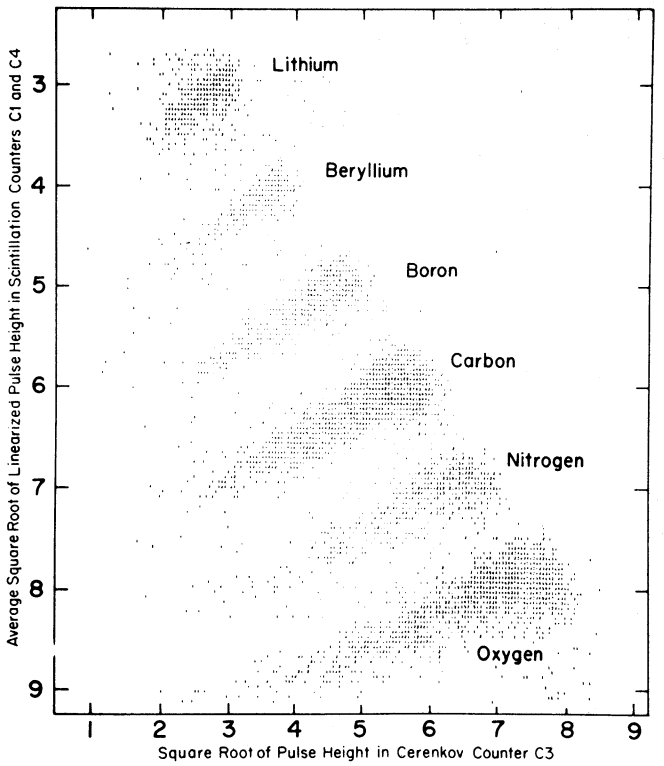

FIG. 4.—Scintillator Cerenkov matrix for the data selected from fig. 3

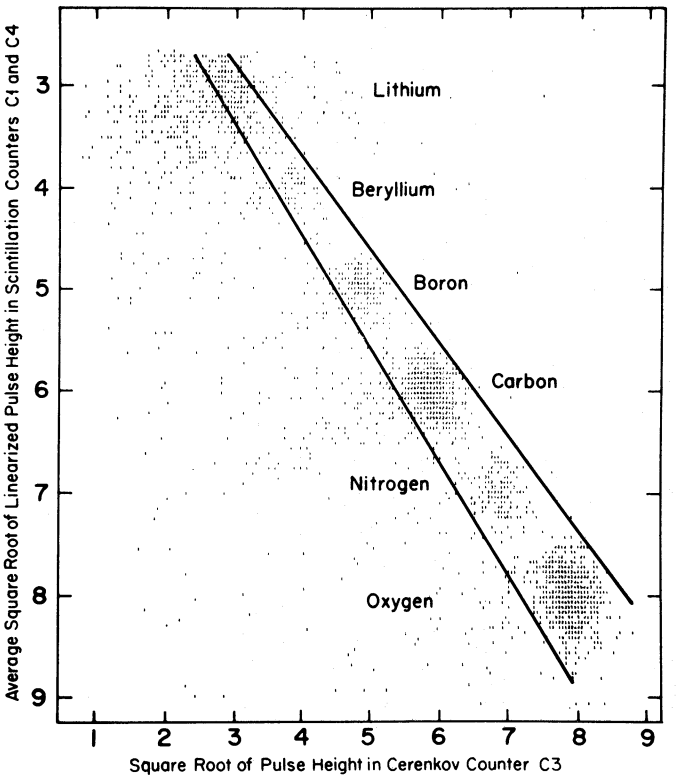

FIG. 5.—Scintillator Cerenkov matrix for data triggering the C2B gas counter in flights 2 and 3. Selection criteria used at high energy, accept only data between the two lines.

unrelated events triggering the gas counter. First, while nonnuclear background seems virtually absent at low energies (fig. 4), there is clearly a concentration of background events around the location of lithium and beryllium in the data of figure 5. The background, presumably mostly due to sideshowers, simulates lithium or beryllium by triggering C1 and C4 at a minimum level. It can then rather easily fire the gas counter at the same time by one or more particles passing through one of the phototubes. It should be noted in comparing the figures that figure 4 shows 1 hour of data, while figure 5 shows 70 hours of data from flights 2 and 3, and during that time over 10^6 events triggered the instrument. Second, a few nuclei that are clearly classified by the Cerenkov counter C3 as having low energy give a signal in the gas counter. This again is not a total surprise, since it must be remembered that for every high-energy nucleus there are about 60 low-energy nuclei. If only one in 600 of these manages to trigger the gas counter, this will already lead to about 10 percent contamination of the high-energy sample by low-energy nuclei, which is approximately the value observed for oxygen. The mechanism through which the low-energy nuclei trigger the gas counters is not entirely clear, but we believe the most likely cause to be δ-rays that pass through the phototube windows. The background seen in figure 5 can be eliminated by new selection criteria. The charge resolution for lithium and beryllium is sufficiently good to select their charge peaks quite sharply. Also, for the high-energy data presented here, we require that $0.8 < C3/C4 < 1.2$. The approximate location of these selection criteria is shown in figure 5. A number of low-energy nuclei, however, is buried under the high-energy peaks and cannot be removed. These nuclei constitute the background correction that has to be applied, and this correction is greatest for the lighter elements.

Besides these corrections for the event selection, namely the background correction, the selection correction, and the overlap correction, corrections are needed to account for the interaction of nuclei in the instrument, in the solid material above the instrument, and in the atmosphere. The *interaction correction* corrects the measured composition of nuclei that pass through the instrument without interaction, in order to represent the composition above the top of the first counter. The magnitude of this correction depends on the amount of material in the instrument, and can be rather accurately calculated. To correct for interaction in the solid material above the top counter poses a greater problem. We have divided this material evenly between instrument and atmosphere and thus apply only one interaction correction and an *atmospheric correction*. This assumes that half of these interactions will be eliminated by the selection criteria, while the other half will feed down as interactions in the atmosphere. The validity of these two assumptions is questionable, and this correction is thus inaccurate. However, since the total amount of material in the instrument above the top counter is equivalent to only 1.4 g cm^{-2} of air, no large error should be caused by this correction.

The atmospheric correction to the data is not small and not straightforward to calculate. If all the spallation cross-sections are known, it can be calculated as has been done by many observers (Cassé *et al.* 1971; Webber, Damle, and Kish 1972; Smith *et al.* 1973). Corrections used by different experimenters do not agree very well, hence this correction can be a source of considerable systematic error. In order to obtain an experimental handle on these corrections we have flown the instrument at variable altitude. Our preliminary results are shown in table 1, together with values used by other observers. These corrections are additive, i.e., the corrected relative abundance (oxygen = 1000) is obtained by adding the correction to the measured abundance. The corrections are normalized to 1 g cm^{-2} of air. The atmospheric corrections that we decided to use for the data presented in this paper are shown in

TABLE 1

ATMOSPHERIC CORRECTIONS FOR THE RELATIVE COMPOSITION OF COSMIC RAYS

Z	Element	Webber *et al.* (1972)	Cassé *et al.* (1971)	Smith *et al.* (1973)	Experimental Values ($E > 0.5$ GeV per nucleon)	Corrections Used
3	Lithium	−5	...	−10	−14 ± 2	−12
4	Beryllium	−3	− 6	− 9	−12 ± 2	− 8
5	Boron	−9	−14	−13	−16 ± 2	−15
6	Carbon	−4	− 8	− 9	−20 ± 4	−16
7	Nitrogen	−2	− 9	− 4	− 9 ± 2	− 8
8	Oxygen	...	...	...	...	...
9	Fluorine	−1	− 1	− 2	...	− 2
10	Neon	0	− 1	− 1	...	0
11	Sodium	−1	− 1	− 1	...	− 1
12	Magnesium	+ 1	0	1	...	+ 1
13	Aluminum	0	0	0	...	0
14	Silicon	+2	2	1	...	+ 2
15–25	VH nuclei*	−1	(1)	− 1	...	0
26	Iron	+4	...	3	...	+ 4

NOTE.—Correction to be added to measured abundance relative to oxygen (oxygen = 1000) to correct for 1.0 g cm^{-2} of overlaying atmosphere.

* Very heavy nuclei.

the last column of tables 1 and 4, and on each figure separately. These are based on averaging the numbers shown in table 1, giving greatest weight to our experimental values and to the corrections used by Smith *et al.* (1973). Details on the experimental determination of the atmospheric corrections will be published elsewhere.

b) Charge Determination

A one-dimensional charge function is obtained from the matrix in figure 4 by summing along straight lines, since the individual charges are empirically found to lie very closely on straight lines in this graph. The slope of the lines varies with Z due to the energy dependence of the nonlinearity of the scintillation material Pilot Y. The pulse heights from the scintillation counters are linearized for the minimum ionizing particles, but the signal from the lower-energy particles is more nonlinear. This is shown in figure 6, where the ratio of the light output over Z^2 for different charges is plotted. This ratio is normalized to 1.0 for minimum ionizing protons. Although there is considerable nonlinearity in the signal, the shape of the response curve allows good charge resolution up to iron. We estimate that our linearization is accurate to 0.2 percent and since the straight line is a very good approximation to the actual charge positions in figure 4, the location of each charge is found to vary less than 0.5 percent with energy.

To separate the individual charges one can count as nuclei of charge Z (Z, integer) all those nuclei whose *measured charge* Z_m lies in the interval $Z \pm 0.5$. The measured abundances of that charge $N_m(Z)$ can then be corrected for the charge overlap, e.g., by

$$N(Z) \simeq \frac{N_m(Z) - \rho\{N_m(Z) + [N_m(Z+1) + N_m(Z-1)]/2\}}{1-2\rho} . \quad (4)$$

Here $\rho = \rho(Z)$ is the overlap fraction, i.e., the fraction of nuclei of charge Z whose measured charge Z_m lies outside the interval $Z \pm 0.5$. Equation (4) is not exact, but it gives in almost all cases a very accurate value for the overlap correction and its error. For greater accuracy unfolding techniques can be used, namely,

$$N(Z) = \sum_{Z'} P_{ZZ'}{}^{-1} \times N_m(Z') . \quad (5)$$

$P_{ZZ'}$ is the probability that a nucleus of charge Z' has a measured charge in the interval assigned to Z.

While it is reasonable to assign the charge interval $Z \pm 0.5$ to the charge Z, the value 0.5 is somewhat arbitrary and any other number could be used. In this analysis, we have for most charges used the selection criteria $Z_o \pm 0.375$ for the odd integer charges and $Z_e \pm 0.625$ for the even integer charges to minimize the overlap correction. To give some idea about the degree of overlap, or the magnitude of the overlap correction, we show in figure 7 the value of N/O one would expect to measure assuming the true ratios of C:N:O:F to be 110:27:100:0. The two curves in the figure show the measured ratio versus charge resolution for the two discussed selection criteria, $Z \pm 0.5$ for each charge (curve *a*) and $Z_o \pm 0.375$ for the odd charges, $Z_e \pm 0.625$ for the even charges (curve *b*). Using the latter criteria, one sees that the overlap correction is zero not only for perfect charge resolution $\sigma = 0$ but also for $\sigma \simeq 0.35$ charge units, and the correction is less than 5 percent up to a charge resolution $\sigma \simeq 0.4$. For the high-energy measurements reported here the charge resolution is better than or equal to 0.4 charge units for all charges, and in the charge region between silicon and iron the statistical accuracy is much less than the magnitude of the overlap correction. Consequently this correction has been ignored in the data presented here. We emphasize that, since the selection criteria are arbitrary, a large overlap

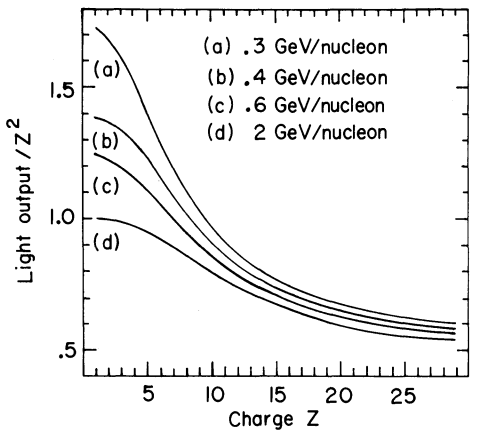

FIG. 6.—Nonlinearity observed in the Pilot Y scintillation material, as a function of energy and charge.

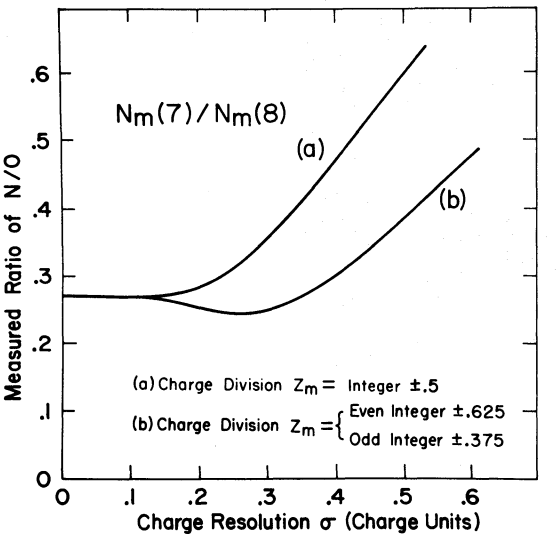

FIG. 7.—Measured ratio of nitrogen to oxygen as a function of charge resolution, using two different selection criteria. True ratio of C:N:O:F are assumed to be 110:27:100:0.

(poor resolution) does not necessarily lead to large overlap corrections, but it leads to inaccurate corrections. For the particular odd-even ratio shown in figure 7, the error on the overlap correction for the odd elements is about double the statistical error, if the charge resolution is 0.4 charge units. This assumes that one knows the exact mean location of each charge and the exact charge resolution.

c) *Energy Determination*

Cerenkov counters are very suitable to measure energy. In the region just above the threshold energy the light output as shown by equation (1) is strongly energy dependent, which allows energy measurements with high resolution. Many different parameters or functions can be used for the energy measurement. The most important one of these that we have used is the pulse height in the Cerenkov counter C3, or $C3/Z^2$, where Z is the determined integer charge of the nucleus. It gives the best energy resolution for nuclei of lower charges and for the higher charges its distribution for a constant energy is not strongly charge dependent since it is determined mostly by the path-length distribution in C3. The theoretical value of this parameter for each energy is accurately known and the parameter is independent of the linearization needed for the scintillators. Another important parameter is C3/C4, i.e., the ratio of the pulse height in the Cerenkov counter to the pulse height in the lower scintillation counter. This parameter is independent of the angle of incidence and therefore gives the best energy resolution for the higher charges. It does not require charge determination and the energy measurement therefore is not subject to error due to misassigned charge. On the other hand, the connection between the energy and the value of this parameter is not as accurately known as for the parameter $C3/Z^2$ and it becomes ambiguous at the highest energies due to the relativistic rise of the C4 output. It is also sensitive to interactions in the bottom counter, C4. We shall call the possible error in relating the measured parameter to energy, the *systematic error* in the energy measurement.

The energy resolution is quite good at low energies and allows the selection of well-defined energy bins. We can further assume that the systematic error is small, since equation (1) applies with great accuracy, and the gas counters can be used to find the value of the parameter that corresponds to infinite energy. Also, the distribution of the pulse heights at a given energy is well known.

Above 20 GeV per nucleon the energy is obtained from the signals produced in the gas Cerenkov counters. The parameters that we have used exclusively are $C2A/Z_m^2$ and $C2B/Z_m^2$, where C2A and C2B are the linearized pulse heights in the two gas Cerenkov counters and Z_m is the measured charge of the nucleus (Z_m is not an integer). The resolution is good close to the threshold, but deteriorates for energy measurements much above the threshold until a maximum energy, approximately given by equation (2), is reached. For the purpose of measuring the energy spectrum the systematic errors in the energy determination are no longer small but become as important as the statistical abundance errors. This is basically due to a lack of calibration. One can assume that equation (1) applies exactly, but an accurate calibration of at least one point is needed. The pulse height corresponding to infinite energy is thus not known, but has to be determined from the data. Also, the contribution of scintillation light in the white gas counter C2A is not known prior to flight and also has to be obtained from the data themselves. This scintillation amounts to about 15 percent of the maximum Cerenkov signal for CO_2 and to about 5 percent for the SF_6 + methane mixture. Finally, the pulse-height resolution of the focusing counter C2B is poor and not well known.

Details of the unfolding procedure to obtain the energy distribution from the measured pulse-height distribution will be described in the Appendix.

IV. RESULTS

a) *Raw Numbers*

The chemical composition above 20 GeV per nucleon is obtained, using the selection criteria that were described in the last chapters. The nuclei are sorted into charge bins according to the selection criteria $Z_m = 3 \pm 0.18$ for lithium,[1] $Z_m = 4 \pm 0.32$ for beryllium,[2] $Z_m = Z_o \pm 0.375$ for the odd elements, $Z_m = Z_e \pm 0.625$ for the even elements, and $Z_m = Z_c + 0.125 \pm 1.0$ for iron and nickel, where Z_o, Z_e, and Z_c are the appropriate integral numbers.

The elimination of the nuclei below 20 GeV and the selection of the remaining nuclei into energy bins is accomplished by divisions of the gas Cerenkov counter outputs according to the guidelines presented in the last section and in the Appendix.

The resulting raw numbers are shown in table 2. To obtain the composition from these raw numbers we have to apply the five corrections that we have previously discussed: (1) overlap correction, (2) background correction, (3) selection correction, (4) interaction correction, and (5) atmospheric correction.

We do not apply any charge overlap correction since its magnitude should be much smaller than the statistical error. One should note, nevertheless, that due to the charge overlap the division between manganese and iron is inaccurate, and for most purposes it will not be advantageous to separate the two. For the same reason no separate charge interval is assigned to cobalt ($Z = 27$).

The background correction is small enough to be ignored for the energy range where both gas counters measure the energy. For the energy range where only

[1] It must be emphasized that selection criteria which take advantage of the clustering of the charges around the theoretical *integral* values are natural and helpful in eliminating background. It is meaningless and misleading, however, to display the "charge resolution" *after* such criteria have been applied, as is sometimes done.

[2] See n. 1.

TABLE 2

NUMBER OF NUCLEI SATISFYING SELECTION CRITERIA, AND CORRECTIONS

MEDIAN ENERGY BIN EDGES, GeV/n	22 GeV/n 20	27 GeV/n 24	34 GeV/n 30	48 GeV/n 40	75 GeV/n 60	120 GeV/n 80	SELECTION CORRECTION	INTERACTION CORRECTION
Lithium	31 (11)	46 (16)	24 (14)	13	6	2	2.30	0.93
Beryllium	30 (15)	35 (17)	23 (16)	11	10	1	1.09	0.95
Boron	67 (44)	66 (43)	47 (38)	23	24	7	1.04	0.97
Carbon	285 (214)	308 (230)	258 (219)	171	102	26	1.02	0.98
Nitrogen	63 (50)	76 (61)	51 (46)	32	27	4	1.01	0.99
Oxygen	238 (202)	289 (245)	252 (239)	196	142	37	1.00	1.00
Fluorine	9	5	5	3	2	1	1.00	1.01
Neon	31	34	35	38	15	2	1.00	1.02
Sodium	2	7	9	6	6	0	1.00	1.03
Magnesium	26	68	37	28	26	6	1.00	1.04
Aluminum	6	8	9	2	3	2	1.00	1.05
Silicon	14	35	38	33	28	6	1.00	1.06
Phosphorus	0	1	1	2	2	0	1.00	1.07
Sulfur	4	8	6	9	3	0	1.00	1.08
Chlorine	2	1	3	0	0	0	1.00	1.09
Argon	2	0	3	8	2	0	1.00	1.11
Potassium	1	5	1	1	0	0	1.00	1.12
Calcium	2	2	9	5	0	0	1.00	1.13
Scandium	0	2	0	0	2	1	1.00	1.14
Titanium	2	2	3	1	2	0	1.00	1.15
Vanadium	0	3	1	2	5	0	1.00	1.16
Chromium	0	1	2	5	3	0	1.00	1.17
Manganese	4	4	3	3	2	0	1.00	1.18
Iron	11	21	30	17	20	6	1.00	1.19
Nickel	2	1	2	2	2	0	1.00	1.21

one gas counter triggers, this correction is a major one. To estimate the correction, certain assumptions must be made. The background under the lithium peak can be estimated from the background in the immediate neighborhood of the peak. To estimate the contamination from low-energy particles, we have made the assumption that the probability of a low-energy particle triggering the gas counter is independent of its energy. We estimate the correction to be known to within 25 percent, but we must admit the potential possibility of introducing a systematic error with these corrections. Application of the background correction leads to the numbers given in parentheses in table 2.

The selection correction can be easily calculated from the known response and resolution of each counter, and is shown in table 2 in the first column under corrections. The correction is large for lithium since this element was not counted with full efficiency in flight 1 and almost completely excluded in flight 3.

The interaction correction is shown in the last column of table 2. From the knowledge of the nuclear interaction lengths and the amount and composition of matter in the instrument, this correction can be calculated rather accurately. It can also be obtained from the data themselves (see, for instance, fig. 3). The corrections in table 2 are multiplicative, i.e., corrected numbers are obtained by multiplying the measured numbers with the correction. They are designed to correct the abundance relative to oxygen, which means that there is no correction (corr. = 1.00) for oxygen. Absolute values of these corrections are given in table 3.

For the purpose of calculating the energy spectra of the different nuclei, table 3 shows the number of oxygen nuclei measured above each energy division, corrected for the background. It includes, furthermore, corrections to be applied because of the imperfections in the energy division. These corrections are the energy overlap correction (see Appendix) and the correction that takes care of the energy dependence of the selection. This last correction takes into account that the lowest energy bin has not been included in flight 1,

TABLE 3

NUMBER OF OXYGEN NUCLEI MEASURED ABOVE EACH ENERGY DIVISION, AND CORRECTIONS

PARAMETER	ENERGY (GeV per nucleon) 20 ± 1.5	24 ± 2	30 ± 3	40 ± 4	60 ± 6	80 ± 10
Number	1061	859	614	375	179	37
Overlap correction	1.00	1.00	1.00	1.02	1.12	2.4
Energy selection correction	1.09	1.00	1.00	1.01	1.07	1.6

NOTE.—Additional corrections to obtain absolute flux: Selection correction, 1.07; interaction correction, 1.33; atmospheric correction, 1.20. Total collection factor, 7.6 m^2 sr hours.

TABLE 4

RELATIVE ABUNDANCES FOR COSMIC-RAY NUCLEI AT 6.0 g cm^{-2} IN THE ATMOSPHERE

Z	Element	Energy (GeV per nucleon) 22	27	34	48	75	120	1	Atmospheric Correction
3.....	Lithium	0.12 ± 0.10	0.14 ± 0.10	0.13 ± 0.06	0.14 ± 0.04	0.09 ± 0.05	0.12 ± 0.12	0.27	−0.07
4.....	Beryllium	0.08 ± 0.04	0.07 ± 0.04	0.07 ± 0.03	0.06 ± 0.02	0.07 ± 0.03	0.03 ± 0.05	0.15	−0.05
5.....	Boron	0.22 ± 0.06	0.18 ± 0.05	0.16 ± 0.04	0.12 ± 0.03	0.17 ± 0.04	0.19 ± 0.09	0.39	−0.09
6.....	Carbon	1.06 ± 0.12	0.94 ± 0.12	0.92 ± 0.09	0.87 ± 0.07	0.72 ± 0.08	0.70 ± 0.15	1.17	−0.10
7.....	Nitrogen	0.25 ± 0.05	0.25 ± 0.04	0.19 ± 0.04	0.16 ± 0.03	0.19 ± 0.04	0.11 ± 0.07	0.33	−0.05
8.....	Oxygen	1.00 ± 0.10	1.00 ± 0.09	1.00 ± 0.07	1.00 ± 0.07	1.00 ± 0.09	1.00 ± 0.18	1.00	...
9.....	Fluorine	0.04 ± 0.02	0.02 ± 0.01	0.02 ± 0.01	0.02 ± 0.01	0.01 ± 0.01	0.03 ± 0.05	0.03	−0.01
10.....	Neon	0.16 ± 0.03	0.14 ± 0.03	0.15 ± 0.03	0.20 ± 0.03	0.11 ± 0.03	0.06 ± 0.05	0.16	0.00
11.....	Sodium	0.01 ± 0.01	0.03 ± 0.01	0.04 ± 0.02	0.03 ± 0.02	0.04 ± 0.02	0.00 ± 0.03	0.04	−0.01
12.....	Magnesium	0.14 ± 0.03	0.29 ± 0.04	0.16 ± 0.03	0.15 ± 0.03	0.19 ± 0.04	0.17 ± 0.09	0.20	+0.01
13.....	Aluminum	0.03 ± 0.02	0.03 ± 0.02	0.04 ± 0.02	0.01 ± 0.01	0.02 ± 0.02	0.06 ± 0.06	0.04	0.00
14.....	Silicon	0.07 ± 0.02	0.15 ± 0.03	0.17 ± 0.03	0.18 ± 0.04	0.21 ± 0.04	0.17 ± 0.09	0.15	+0.01
15–24....	VH nuclei	0.07 ± 0.02	0.12 ± 0.02	0.14 ± 0.03	0.19 ± 0.04	0.15 ± 0.04	0.03 ± 0.05	0.16	0.00
25–28....	Iron group	0.10 ± 0.03	0.13 ± 0.03	0.18 ± 0.03	0.13 ± 0.03	0.20 ± 0.04	0.20 ± 0.10	0.10	×1.20

*Atmospheric correction is additive, except multiplicative correction is used for iron.

due to large background contamination and that the highest energy bin was not included in flight 3. It also takes into account that during the last third of flight 2 the Cerenkov counter C2A was not operating properly, and therefore energy was measured by C2B alone and the last two energy bins were not included. In order to calculate the absolute fluxes of the elements, table 3 also includes the *absolute* value of the selection correction and the interaction correction. Furthermore, it shows the atmospheric correction which we have used and the total collection factor. All corrections in this table are multiplicative.

b) *Relative Composition*

The relative composition is computed from the raw numbers and the corrections shown in table 2. The result is given in table 4. For comparison our measured preliminary abundances at low energy (E = 1.0 GeV per nucleon) are shown in the next to last column. In the last column we show the atmospheric corrections that we have used (see also table 1). These corrections, which should be added to the relative abundance, could be a source of error, and any comparison of our data with those of other observers should include a comparison of the respective atmospheric corrections. The atmospheric corrections given are probably accurate to within ±0.01, or to within ±0.02, for the elements of charge less than oxygen. The individual errors given in the table, which are the statistical errors plus an estimated 25 percent error in the background correction, should consequently not be much affected by the atmospheric correction. If charges or energy intervals are grouped together to reduce the statistical errors, the systematic error on the atmospheric correction may, however, limit the final accuracy.

Some important differences are observed in the composition at high (E > 20 GeV per nucleon) and low (E = 1.0 GeV per nucleon) energy. The most prominent result is the decreasing relative abundance of galactic secondary nuclei as energy increases. We show in figure 8 the ratio of all those nuclear species that are mostly secondary (daughter nuclei) to those that are presumed to be mostly primary (parent nuclei). The results shown in this figure are in good agreement with our published data which were based on the first flight only (Júliusson *et al.* 1972), but slightly lower in the energy range 20–40 GeV per nucleon. This energy range was covered in the first flight using the C2A Cerenkov counter only and the contamination by low-energy nuclei, especially boron, was seemingly larger than we accounted for. The new results, presented in figure 8, show better agreement with those obtained by other observers who have observed a reduced secondary to primary ratio at much lower energies. In figure 8 we have grouped together all parent nuclei and all daughter nuclei in order to obtain the best statistical accuracy and to minimize the danger of possible systematic errors. However, the declining ratio of daughter to parent

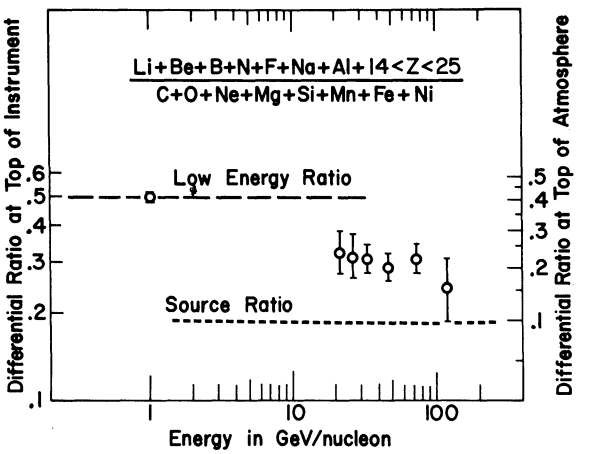

FIG. 8.—Ratio of daughter nuclei to parent nuclei in cosmic rays, as a function of energy. The daughter nuclei are defined to be those nuclear species that are mostly produced by spallation. Broken line indicates the value measured at low energy (1 GeV per nucleon), and the dashed line the value expected at the source (Webber *et al.* 1972).

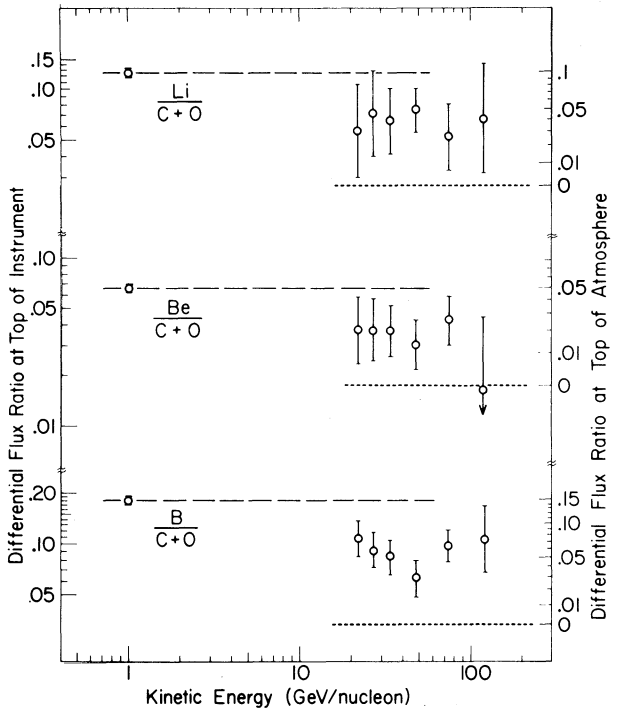

FIG. 9

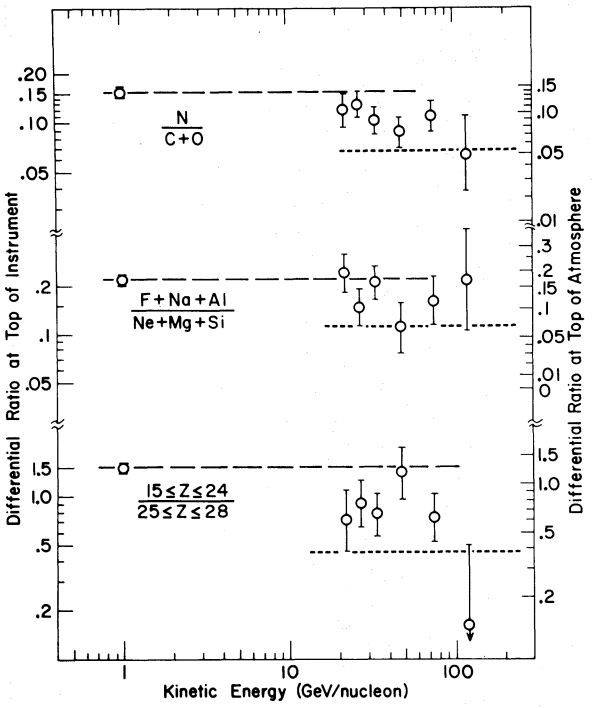

FIG. 10

FIG. 9.—Ratios of the secondary light nuclei to carbon and oxygen in cosmic rays as a function of energy. Broken and dashed lines have same meaning as in fig. 8. Note that the right-hand scale has a form [log (y + const.)] that is asymptotically logarithmic at high values ($y \gg$ const.) but becomes asymptotically linear at low values.

FIG. 10.—Various daughter to parent ratios measured in the cosmic rays as a function of energy. Broken and dashed lines have same meaning as in fig. 8.

nuclei can be observed for the individual species, as we show in figures 9 and 10. In figure 9 the individual light elements are compared with C + O. The decrease of the relative abundance of the light nuclei is clearly seen, but it must be emphasized that the lithium measurements, and to some degree the beryllium measurements, are inaccurate at those energies which are covered by one gas counter only. In particular, the errors on the three lowest energy points are to a great extent due to the systematic error on the background correction. These errors are therefore correlated and the points are not statistically independent.

In figure 10 we show similarly the ratios N/(C + O), (F + Na + Al)/(Ne + Mg + Si), and ($14 < Z < 25$)/Fe as a function of energy. Nitrogen is clearly reduced at high energies to a value close to the source ratio. The ratio (F + Na + Al)/(Ne + Mg + Si) exhibits a measurable drop at higher energies indicating the secondary nature of the (F, Na, Al) nuclei. Finally, we plot the ($14 < Z < 25$)/Fe ratio. The daughter elements in the numerator are mostly secondary products from iron and a decline in the ratio is also seen here.

The reduction of the secondary to primary ratio which we present here must be explained as a decrease in the probability of spallation of the primary nuclei at high energies. Other features, possibly unrelated, can also be observed. In figure 11 we show the C/O ratio measured as a function of energy. This result has been published (Júliusson and Meyer 1973), using slightly different selection criteria and atmospheric correction. If the secondary to primary ratio changes, some reduction of the C/O ratio with increasing energy is expected due to the contribution of secondary carbon. We would, therefore, expect to measure at high energies a value closer to the source ratio. As seen in the figure, the ratio at high energies has a value considerably below the expected source ratio. Unless the source ratio is substantially overestimated, our data indicate that the source composition of carbon and oxygen is energy dependent and the source that contributes to the high-energy particles is richer in oxygen.

The same figure also shows our measured Fe/(C + O) ratio as a function of energy. Again we expect a value closer to the source ratio, due to the decrease of spallation of iron at high energies, but also in this case the change that we observe is greater than expected and, at the highest energy, the ratio is somewhat above the calculated source ratio. This could be due to an underestimate of the source ratio or it might again point toward a change in source composition at high energy. The figure also shows our measured (Ne + Mg + Si)/(C + O) ratio. The source ratios shown by the dashed lines in figures 8 to 11 were taken from Webber *et al.* (1972). They are the result of an

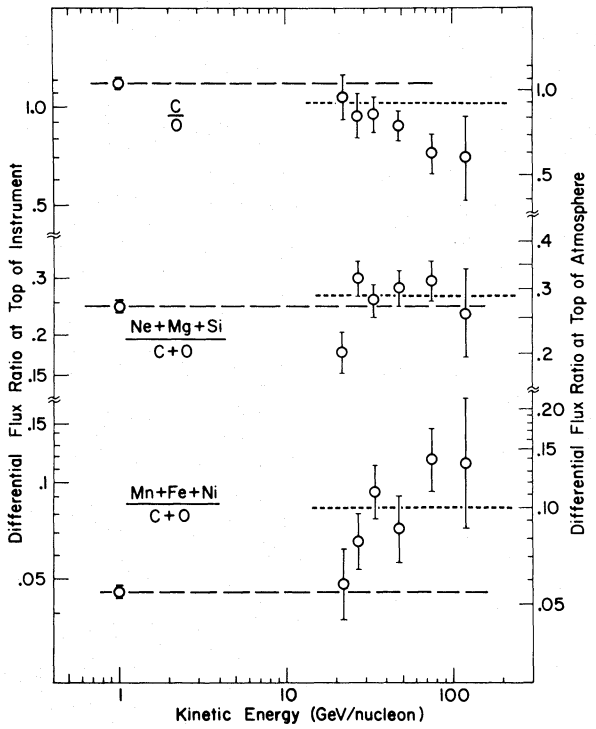

FIG. 11.—Ratios of various parent nuclei in the cosmic rays as a function of energy. Broken and dashed lines have same meaning as in fig. 8.

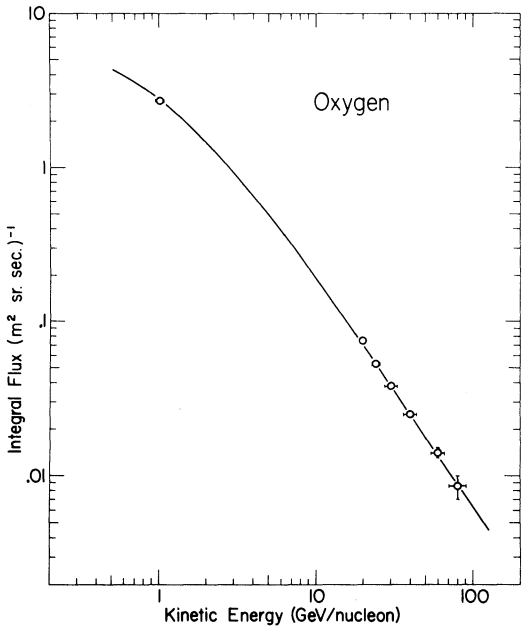

FIG. 12.—Integral energy spectrum of oxygen in the cosmic rays. The line represents a spectrum in total energy of the form $N(E) = 7.5(E_{\text{tot}})^{-1.53}$ particles $m^{-2}\,sr^{-1}\,s^{-1}$ (E in GeV per nucleon).

extrapolation of the observed low-energy abundances to the sources, using a transport equation.

c) Absolute Flux and Energy Spectra

Obtaining the energy spectra of individual elements from our measurements is more difficult than to obtain the relative abundances, or the differences between the spectral indices. Since these differences are small, systematic errors in the energy determination are quite unimportant as long as the energy intervals are the same for each charge. The spectra themselves are an order of magnitude steeper than the spectral differences. Errors in energy are therefore an order of magnitude more important. These systematic errors arise from connecting the energy parameter ($C2/Z_m^2$) to measured energy, and from tying the measured energy to the actual energy. If these systematic errors could be ignored, our statistical accuracy would permit us to determine the spectral index for the abundant elements carbon and oxygen with an accuracy of 0.01, assuming that we can approximate the spectrum with a single power law. The measured integral energy spectrum for oxygen is obtained from table 3 and is shown in figure 12. We have plotted separately our estimated systematic errors in the energy and the abundance errors, which include statistical errors plus 25 percent of the background correction. For computing a best straight-line fit, the energy errors are converted into abundance errors and added to the existing abundance errors. The integral spectrum can be well approximated by a power spectrum in total energy of spectral index 1.53 ± 0.04 from the region of geomagnetic cutoff and up to the maximum energy (*solid line* in fig. 12). The individual kinetic energy ranges 1.0–20 GeV per nucleon and 20–80 GeV per nucleon give separately indices of 1.51 ± 0.04 and 1.59 ± 0.13. We have used a power law in total energy for the spectrum since it fits the data much better than a power law in kinetic energy, and somewhat better than a power law in rigidity.

A table of differential fluxes for individual elements is obtained by differentiating the best power-law fit to the high-energy points in figure 12, and by multiplying the resulting oxygen flux with the abundance of each element relative to oxygen. The resulting values are shown in table 5. The errors are statistical plus an estimated error (25 percent) in the background correction, except the errors on the odd elements above silicon which are twice the statistical error to account for the charge overlap. The error on the absolute value of the differential flux of oxygen at each energy is twofold, and includes firstly the statistical accuracy of the measured number and the systematic error in the energy. Secondly, we have the error in converting the numbers to differential flux. That error is the combined error in the absolute value of the selection correction, interaction correction, atmospheric correction, and the error in the collection factor (shown in table 3). We estimate this last charge- and energy-independent error to be less than 5 percent, and it is included in the estimate of the systematic error in the energy shown at the top of the table.

Table 6 shows the observed spectral indices for

TABLE 5

DIFFERENTIAL FLUX OF COSMIC-RAY NUCLEI (10^3 m^2 sr s GeV per nucleon)$^{-1}$

Z	Element	Energy (GeV per nucleon) 22 ± 2	27 ± 2	34 ± 3	48 ± 5	75 ± 8	120 ± 15
3	Lithium	0.20 ± 0.43	0.18 ± 0.27	0.08 ± 0.09	0.044 ± 0.025	0.004 ± 0.009	+0.003 ± 0.007
4	Beryllium	0.12 ± 0.18	0.06 ± 0.10	0.03 ± 0.04	0.005 ± 0.011	0.005 ± 0.005	−0.001 ± 0.003
5	Boron	0.55 ± 0.24	0.22 ± 0.12	0.11 ± 0.05	0.016 ± 0.016	0.015 ± 0.007	+0.006 ± 0.005
6	Carbon	4.15 ± 0.50	2.18 ± 0.30	1.20 ± 0.12	0.470 ± 0.042	0.121 ± 0.015	+0.035 ± 0.009
7	Nitrogen	0.86 ± 0.22	0.52 ± 0.11	0.21 ± 0.05	0.069 ± 0.019	0.027 ± 0.008	+0.003 ± 0.004
8	Oxygen	4.32 ± 0.41	2.60 ± 0.23	1.46 ± 0.10	0.611 ± 0.045	0.196 ± 0.017	+0.059 ± 0.010
9	Fluorine	0.15 ± 0.07	0.03 ± 0.02	0.02 ± 0.02	0.004 ± 0.007	0.001 ± 0.003	+0.001 ± 0.003
10	Neon	0.68 ± 0.13	0.37 ± 0.07	0.22 ± 0.04	0.121 ± 0.020	0.021 ± 0.007	+0.003 ± 0.003
11	Sodium	0.00 ± 0.04	0.05 ± 0.04	0.04 ± 0.02	0.013 ± 0.010	0.007 ± 0.004	−0.001 ± 0.002
12	Magnesium	0.63 ± 0.12	0.78 ± 0.10	0.25 ± 0.04	0.097 ± 0.018	0.040 ± 0.008	+0.011 ± 0.005
13	Aluminum	0.13 ± 0.07	0.09 ± 0.04	0.06 ± 0.02	0.007 ± 0.007	0.004 ± 0.003	+0.003 ± 0.005
14	Silicon	0.36 ± 0.10	0.42 ± 0.07	0.26 ± 0.04	0.115 ± 0.022	0.043 ± 0.008	+0.011 ± 0.005
15	Phosphorus	0.00 ± 0.04	0.01 ± 0.03	0.01 ± 0.02	0.007 ± 0.012	0.003 ± 0.004	+0.000 ± 0.003
16	Sulfur	0.09 ± 0.06	0.09 ± 0.04	0.05 ± 0.02	0.031 ± 0.012	0.005 ± 0.003	+0.000 ± 0.002
17	Chlorine	0.05 ± 0.08	0.01 ± 0.03	0.02 ± 0.02	0.000 ± 0.005	0.000 ± 0.002	+0.000 ± 0.003
18	Argon	0.05 ± 0.05	0.00 ± 0.02	0.02 ± 0.01	0.027 ± 0.012	0.003 ± 0.003	+0.000 ± 0.002
19	Potassium	0.02 ± 0.04	0.06 ± 0.04	0.01 ± 0.02	0.004 ± 0.008	0.000 ± 0.002	+0.000 ± 0.003
20	Calcium	0.05 ± 0.05	0.02 ± 0.02	0.06 ± 0.02	0.018 ± 0.009	0.000 ± 0.002	+0.000 ± 0.002
21	Scandium	0.00 ± 0.04	0.02 ± 0.03	0.00 ± 0.01	0.000 ± 0.006	0.003 ± 0.005	+0.002 ± 0.003
22	Titanium	0.05 ± 0.05	0.02 ± 0.02	0.02 ± 0.01	0.004 ± 0.006	0.003 ± 0.003	+0.000 ± 0.002
23	Vanadium	0.00 ± 0.04	0.04 ± 0.04	0.01 ± 0.02	0.007 ± 0.009	0.008 ± 0.006	+0.000 ± 0.003
24	Chromium	0.00 ± 0.04	0.01 ± 0.02	0.02 ± 0.01	0.018 ± 0.010	0.005 ± 0.004	+0.000 ± 0.002
26	Iron + manganese	0.47 ± 0.13	0.38 ± 0.08	0.29 ± 0.05	0.087 ± 0.023	0.045 ± 0.010	+0.014 ± 0.007
28	Nickel	0.06 ± 0.06	0.01 ± 0.02	0.01 ± 0.02	0.008 ± 0.008	0.003 ± 0.003	+0.000 ± 0.002

NOTE.—An entry $a + b$ means that our best estimate of the value and its 1 σ upper limit are a and $a + b$, respectively; $a^2/(a + b)$ is usually a better estimate for the 1 σ lower limit than $a - b$.

TABLE 6

SPECTRAL INDICES MEASURED FOR COSMIC RAYS

Z	Element	At 6.0 g cm^{-2} in Atmosphere*	At Top of Atmosphere	Above 20 GeV per nucleon
3	Lithium	2.78 ± 0.07	2.95 ± 0.12	2.9 ± 0.8
4	Beryllium	2.80 ± 0.06	3.09 ± 0.14	3.2 ± 0.7
5	Boron	2.80 ± 0.04	2.95 ± 0.07	2.8 ± 0.4
6	Carbon	2.63 ± 0.02	2.65 ± 0.02	2.9 ± 0.2
7	Nitrogen	2.71 ± 0.04	2.74 ± 0.03	3.1 ± 0.3
8	Oxygen	...	2.53 ± 0.02	2.6 ± 0.1
9	Fluorine	2.62 ± 0.08	2.67 ± 0.10	3.3 ± 0.6
10	Neon	...	2.57 ± 0.03	2.9 ± 0.2
11	Sodium	2.63 ± 0.09	2.66 ± 0.10	2.5 ± 0.5
12	Magnesium	...	2.56 ± 0.03	2.7 ± 0.2
13	Aluminum	...	2.61 ± 0.08	2.6 ± 0.5
14	Silicon	...	2.50 ± 0.03	2.2 ± 0.2
15	Phosphorus	...	2.6 ± 0.3	
16	Sulfur	...	2.6 ± 0.1	
17	Chlorine	...	2.7 ± 0.3	
18	Argon	...	2.5 ± 0.1	
19	Potassium	...	2.7 ± 0.3	
20	Calcium	...	2.7 ± 0.1	2.5 ± 0.3
21	Scandium	...	2.5 ± 0.3	
22	Titanium	...	2.7 ± 0.1	
23	Vanadium	...	2.4 ± 0.3	
24	Chromium	...	2.6 ± 0.1	
26	Iron + manganese	...	2.39 ± 0.04	2.2 ± 0.2
28	Nickel	...	2.3 ± 0.2	...

* Corrected for the energy loss, but not for spallation in the atmosphere. Only statistical errors are shown. A systematic error of ±0.1 should be included, applying equally to all elements. Spectra have been fitted to a power law in total energy.

different elements. Only statistical errors are included in the table. These errors should be valid for individual spectral differences, but a systematic error in the absolute index of 0.1 should be included to account for the systematic errors in energy, and the assumption that a single power law can approximate the true spectra. Note that no error is included due to the atmospheric corrections. In particular, the steepness of the beryllium spectrum may be partly caused by too large an atmospheric correction. We used the same corrections at high and low energy, which is reasonable if beryllium is mostly produced by spallation of oxygen. If it is mostly produced by boron, the atmospheric correction should be smaller at high energy. For the results shown in table 6 we assume power laws in total energy for all energies above 1 GeV per nucleon. This differs from the usual assumption that the composition is energy independent up to at least 3 GeV per nucleon. The validity of these assumptions will be discussed further in the next chapter.

V. DISCUSSION

a) Experimental Results

The measurements reported in this paper show clearly that secondary nuclei are reduced at high energy with respect to primary or source nuclei. Only a limited energy interval is covered, namely 20–120 GeV per nucleon, and hence it is difficult to determine precisely the functional form of the energy dependence of the secondary to primary ratio (hereafter called S/P ratio) within that interval. In order to explain these measurements, one must investigate how they fit into a larger picture of cosmic-ray composition over a wide energy range.

Since earlier measurements were usually interpreted as showing an energy-independent composition, one might interpret the results as showing the S/P ratio to be energy independent up to a certain energy, above which the energy spectra of the secondary nuclei become steeper than the energy spectra of the primary nuclei. Alternatively, one could assume that the S/P ratio changes gradually with energy. To clarify this point experimentally we show in figure 13 results by various observers on the (B + N)/C ratio. Since all of boron and most of nitrogen are secondary, while most of carbon is primary, this ratio should show an energy dependence similar to the S/P ratio, although smaller. At the same time charge-dependent effects, including charge-dependent systematic errors, should be minimized since (B + N) has the same average charge as carbon. We have included our own, although preliminary, data at low energies. All measurements are shown as differential points. If integral measurements have been reported, we have tried to estimate the differential equivalent, or the median energy of the sample the point is based on. A smooth variation of the S/P ratio with energy is in good agreement with the data in figure 13, but a break at some energy below a few GeV per nucleon cannot be excluded. Our measurements are in good agreement with an energy dependence of the ratio described by a power law in total energy: $(\mathrm{B} + \mathrm{N})/\mathrm{C} = 0.65 E_{\mathrm{tot}}^{-0.20}$.

b) Interpretation in Terms of an Energy-dependent Production Cross-Section

A possible explanation of the observed change in the S/P ratio may be sought in a change of the production cross-sections for the secondary nuclei at high energy. Either the primary nuclei interact less at high energy or they break up differently after an interaction. We can test this possibility experimentally by looking at nuclei that interact in the instrument.

On the basis of our data and of results obtained on accelerators at energies up to 300 GeV per nucleon (Katcoff *et al.* 1973), we conclude that the observed decrease in the abundance of secondary nuclei with respect to primary nuclei is not caused by a change in the interaction cross-sections or the fragmentation

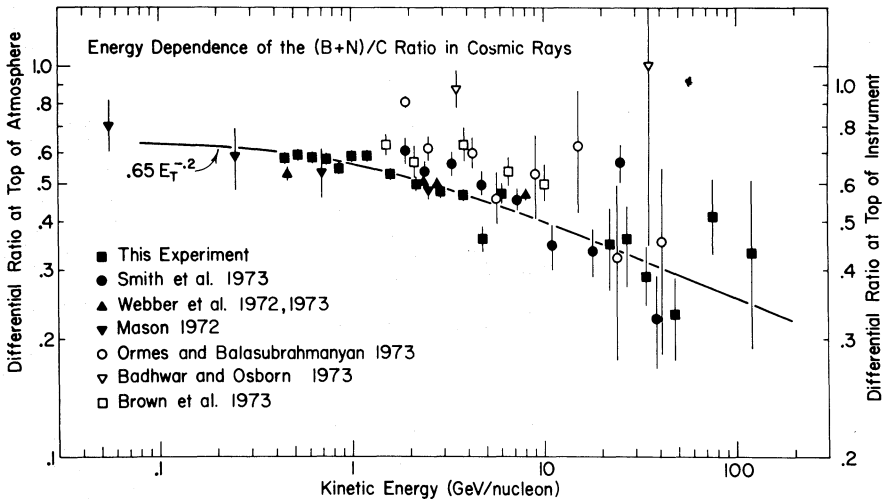

FIG. 13.—Ratio of boron plus nitrogen to carbon measured as a function of energy by various observers

parameters. This experimental conclusion is also in agreement with theoretical predictions.

c) *Interpretation in Terms of Energy-dependent Path-Lengths*

Since the observed change in the S/P ratio cannot be explained by changing production cross-sections, this change must be due to a reduced amount of matter that the cosmic rays have traversed. In other words, the mean path length λ (in g cm^{-2}) must be decreasing as the energy of the particles increases. Such an interpretation has been discussed in several papers (Audouze and Cesarsky 1973; Cesarsky and Audouze 1973*a*, *b*; Meneguzzi 1973*a*, *b*) and we shall mention only a few of the ideas presented. If the energy dependence of λ does undergo an abrupt change at some energy, one would expect an abrupt change in the slope of both the primary and the secondary particle spectra, provided the secondary nuclei are produced rather uniformly throughout the Galaxy, and an energy-dependent leakage lifetime in the Galaxy can be defined. Such a break is not observed by us (fig. 12), although we cannot claim on the basis of our data that a break does not exist. No such break has been reported for the helium, proton, or electron spectra (Webber 1974). It should be noted, however, that if such a break occurs below a few GeV per nucleon, it would be difficult to observe due to the effects of solar modulation, even if one knew the original source spectra.

If the primary cosmic rays were extragalactic, or if the secondary nuclei are not produced uniformly in the Galaxy, a break in λ might not cause a break in the primary spectra. The bulk of the secondary cosmic rays could be produced in a gaseous envelope surrounding the source, in interstellar clouds of higher density of matter and magnetic field, or even within the solar system (Kegel 1973; Cartwright 1973; Cowsik and Wilson 1973; Rengarajan, Stephens, and Verma 1973). In agreement with our results, we shall assume that no sudden change in the energy dependence of λ occurs. For the purpose of this discussion we describe the energy dependence of λ by a power law in total energy $\lambda(E) = \lambda_0 E_{\rm tot}{}^{-\alpha}$. In the case of propagation through a thin slab of matter, $\lambda(E)$ would show the same energy dependence as the S/P ratio. If the path lengths have an exponential distribution with a mean λ_e, it would be equivalent to a different and charge-dependent slab thickness λ_s with $\lambda_s{}^{-1} = \lambda_e{}^{-1} + \lambda_{\rm int}{}^{-1}$, where $\lambda_{\rm int}$ is the interaction mean free path for a particular charge (Cowsik *et al.* 1967). Therefore, if the S/P ratio can be described by a power law in total energy of exponent $-\alpha$ ($\alpha = 0.4$ fits our data best), then a best power law for $\lambda(E)$ might have a different and larger exponent. We shall not try to predict the energy dependence of $\lambda(E)$ that best fits our data in any particular propagation model, but we propose that a power law in total energy would be a simple description to account for the experimental evidence.

If the propagation is described by an energy-dependent lifetime in the Galaxy, say $\tau(E) = \tau_0 E_{\rm tot}{}^{-\alpha}$, one notes that the spectra of the primary nuclei one observes at Earth have been steepened by the propagation, and flatter injection spectra are needed at the sources. Since α seems to be of order 0.3–0.5 one will require a considerably larger energy input from the sources than has previously been estimated. The steepening of the equilibrium spectra has been used to explain the absence of a break in the electron spectrum due to the synchrotron and inverse Compton losses (Silverberg and Ramaty 1973; Júliusson *et al.* 1973). In this picture the high-energy electrons are young and have not yet suffered serious radiative losses.

The picture of propagation which uses only one parameter, namely an energy-dependent residence lifetime in the Galaxy, may not be the right one. The model of Cowsik and Wilson (1973), in which secondary nuclei are produced near the sources, is appealing for two reasons. First, it avoids the requirements of increased power in the sources for cosmic-ray production. Second, an energy dependence of λ in the energy region which we are observing could be readily explained by magnetic irregularities of scale length comparable to the cyclotron radii of the nuclei at those energies. On the other hand, if most secondary nuclei are produced near the source, less matter has to be traversed in the Galaxy. This can be achieved only if either the lifetime of the particle in the Galaxy is shorter or if the average density of matter in the Galaxy is lower than usually assumed.

d) *Other Interpretations*

The observed change in the S/P ratio can be explained by postulating different sources or different source composition for the high-energy cosmic rays, and that nuclei from these sources have a shorter path length than the nuclei arriving from the low-energy sources. Such an interpretation is not necessary to explain the change in the S/P ratio, but may be necessary to explain the observed change in the C/O and Fe/(C + O) ratio, as proposed by Ramaty, Balasubrahmanyan, and Ormes (1973). The energy variation of both these ratios does not agree well with a charge-independent injection spectrum and subsequent energy-dependent propagation. We do not, however, presently know the accuracy of the source ratios that are shown by the dashed lines in figures 8–11. These source ratios are calculated (Webber *et al.* 1972) using energy-independent propagation and the use of an energy-dependent λ may affect the result. Secondly, the production cross-sections used to calculate the source ratios are inaccurate. Only a few of these cross-sections are known experimentally, most of them being obtained from model calculations. For extrapolating the C/O ratio back the source the production cross-section of carbon from collisions of oxygen is important, but this cross-section has not been measured. To explain the observed variation in the C/O ratio by propagation alone would require a revision of the source value of C/O from 0.9 to less than 0.7. This would involve a considerable revision

of the production cross-sections, but it would bring the C/O ratio at the cosmic-ray source into better agreement with the value observed in the solar-system abundances. The required change in the source ratio of Fe/(C + O) is not a major one, particularly if the source abundance of carbon is reduced. Furthermore, if the path length λ at any particular energy is determined from the boron abundances which yields the best accuracy for λ, it will be very important for determining the source ratio of Fe/(C + O), whether the path length has an exponential distribution or not. In conclusion, the uncertainties in the source ratios, as well as in the measurements reported here prevent us from claiming that new sources are needed to explain our observations. The values of the C/O and the Fe/(C + O) ratios and their variation above 20 GeV per nucleon, however, strongly suggest this possibility. One should note that by new sources we do not necessarily mean physically separate sources, but simply that the source composition at high energy is not the same as at low energy. The injection spectra of the different nuclei are then different for individual source nuclei, flattening with increasing charge. One notes from table 6 that the spectral index for the source elements Ne, Mg, and Si is not flatter than that for oxygen, but after a calculation of these spectra back to the source it may be that an injection spectral index that flattens rather smoothly with charge is applicable. Our measured spectrum for iron is steeper than reported by Ormes and Balasubrahmanyan (1973) and we cannot support their conclusion that iron would, aside from hydrogen and helium, be the most abundant element in the cosmic rays above 200 GeV per nucleon. However, the iron spectrum reported here is flatter than that of any other nuclei, and if that difference persists to still higher energies iron would eventually become the dominant component in the cosmic rays.

The author wishes to express his gratitude to his faculty sponsor, Professor Peter Meyer, for his continuous support throughout the course of this work and for many valuable discussions and useful suggestions. He is indebted to Professor Dietrich Müller for many contributions. The project's electronics engineer was Harold Boersma, assisted by Dan Hunsinger, William Hollis, and Gary Kelderhouse. Mechanical design and construction of the instrument were performed by Wayne Johnson and Anthony Kittler. Data analysis programs have been written by Linda Glennie and Leigh Littleton. Valuable contributions from John Caldwell, who participated in many aspects of this work, and discussions with Professor Jacques L'Heureux are greatly appreciated. The author expresses his thanks for generous support from the Icelandic Science Foundation. The balloon flights were conducted under the U.S. Navy Project Skyhook, and by the staff of the National Scientific Balloon Facility (National Center for Atmospheric Research).

APPENDIX

UNFOLDING OF THE ENERGY MEASUREMENTS

The basic quantity that we wish to measure is $N(\Delta E)$, the true number of nuclei in the energy interval ΔE. The quantity $N(\Delta E) = \int_{\Delta E} n(E)dE$, where $n(E)$ is the differential energy spectrum. We shall let $N(E)$ denote the integral form of the spectrum $N(E) = \int_E^\infty n(E)dE$. As was done in the case of charge measurements, we select and determine the number of nuclei that fall into a certain range of measured energy $N_m(\Delta E_m)$. However, in contrast to the charge measurement, the approximation that the nuclei within ΔE_m are all within ΔE is never perfect since the energy spectrum is continuous and there will always be some overlap between the energy intervals. The approximation $N_m(\Delta E_m) = N(\Delta E)$ will be accurate if the energy resolution is much better than the width of the interval ΔE, but to obtain a better measure for $N(\Delta E)$ we shall apply a multiplicative overlap correction on the measured number, $N(\Delta E) = N_m(\Delta E_m) \times$ correction.

Defining the connection between E_m and E by using for E the median energy of those nuclei whose measured energy is E_m, we now need a method to determine the overlap correction. Our method of obtaining the corrections is somewhat different from the unfolding indicated by equation (5). We assume or guess some form for $n(E)$, for example, a power law with some spectral index. Call that spectrum $n^g(E)$, from which the number $N^g(\Delta E) = \int_{\Delta E} n^g(E)dE$ can be determined. By folding in the instrumental response and resolution we obtain the number that we would expect to measure $N_m{}^g(\Delta E_m)$ and we use the ratio of the two numbers as correction. In other words

$$N(\Delta E) = N_m(\Delta E_m) \times N^g(\Delta E)/N_m{}^g(\Delta E_m)\,, \quad \text{(A1)}$$

$$N(E) = N_m(E_m) \times N^g(E)/N_m{}^g(E_m)\,, \quad \text{(A2)}$$

$$n(E) = N_m(\Delta E_m) \times n^g(E)/N_m{}^g(\Delta E_m)\,. \quad \text{(A3)}$$

The main reason for using this method, rather than solving the unfolding equation (5), is its simplicity. The resulting corrections are only weakly dependent on the spectral form $n^g(E)$, and one need not correct the relative abundance measurements, since the corrections are virtually charge independent. Also, in contrast to unfolding, the method can equally well correct integral measurements, as shown by equation (A2) and one need not determine $N(\Delta E)$ first and then divide by ΔE to find $n(E)$, but one can just as easily determine $n(E)$ directly, as shown by equation (A3).

In practice, the overlap corrections and the connection between E_m and E are found by using the first analysis program to generate a data tape of nuclei

having random energy, but with the energy spectrum corresponding to a power law. A pulse height is then computed for each nucleus, and randomized to account for the instrument response and resolution. The resulting tape of "high-energy nuclei" is then analyzed by the second program exactly like the real data. The energy distribution corresponding to ΔE_m, which we call $D(E)$, can be found as well as the corrections for any selection.

We shall now discuss in more detail the connection between the measured energy E_m of a nucleus and its actual energy E. In order to maximize the accuracy in the correction we should define the connection between E and E_m such that the composition in a nuclear sample with the energy distribution $D(E)$ is the same as the differential composition at a value of E that we shall call $E_{\rm diff}$. Here $D(E)$ is the distribution of energies for the sample of nuclei selected by the selection criteria; namely the criteria that the measured energy be within ΔE_m. $E_{\rm diff}$ is then some average energy in the distribution $D(E)$ that we do not know how to calculate, except in the simple case given by equation (3), where $D(E)$ is a power law from $E_{\rm int}$ to infinity. In this paper, instead of $E_{\rm diff}$ we use the median energy of the distribution $D(E)$. If $D(E)$ is a power law above $E_{\rm int}$, $E_{\rm median}$ is a reasonable approximation to $E_{\rm diff}$ but somewhat lower. The mean energy $E_{\rm mean}$ would be a poorer approximation to $E_{\rm diff}$ since it is significantly higher. Except for our highest energy point, there is not much difference between $E_{\rm median}$, $E_{\rm mean}$, and $E_{\rm diff}$. We again emphasize that the connection between E and E_m is to some degree arbitrary. The overlap corrections will depend on the definition of the connection between E and E_m. Whether $E_{\rm mean}$ or $E_{\rm median}$ is used will not lead to systematic differences in the end result.

The connection between the measured and the actual energy is illustrated in figure 14*a*, which shows an idealized situation of energy measurement with a gas Cerenkov counter of threshold energy 20 GeV per nucleon. Its resolution is assumed to be limited only by photoelectron statistics, and the light yield is assumed to be 100 photoelectrons for a nucleus traveling at the speed of light. For simplicity, we choose an energy spectrum $n(E) \propto E^{-3}$ or $N(E) \propto E^{-2}$. An energy spectrum (more exactly, momentum spectrum) of that form would yield a flat pulse-height spectrum from zero to maximum assuming the pulse height is measured with infinite resolution. This spectrum is shown by the solid line in figure 14*a*. The result of actual measurements is represented by the solid line of figure 14*b*, in which the same spectrum is used, after accounting for the finite pulse-height resolution. Figure 14*b* thus shows the spectrum in terms of measured energy. The most obvious difference between the two figures is the number of events whose measured energy lies beyond infinity. One can analyze the pulse height spectrum of figure 14*b* by dividing it into bins as shown by dashed lines in figure 14*b*. These sharp divisions in measured energy will not correspond to sharp divisions in actual energy, but rather to the divisions shown by the dashed lines in figure 14*a*. A

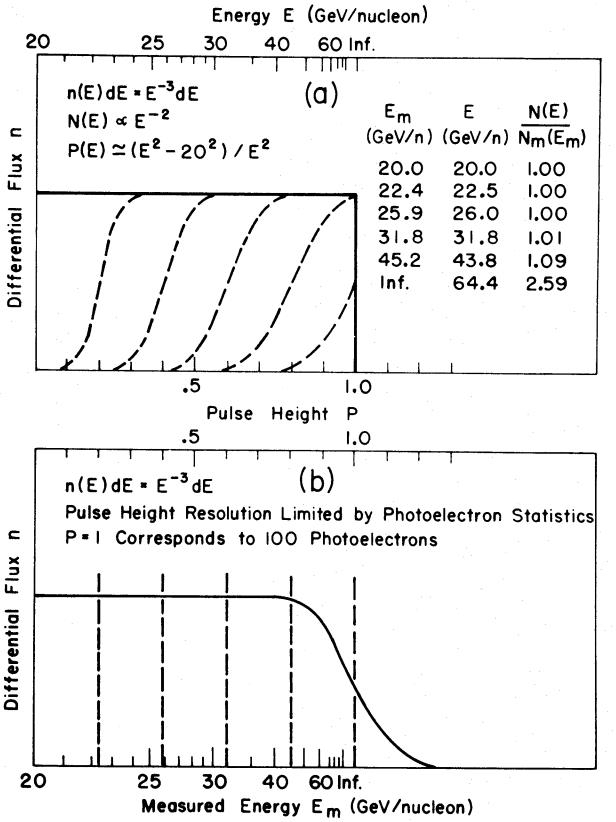

FIG. 14.—Histogram of pulse heights produced in a gas Cerenkov counter by nuclei of differential energy spectrum E^{-3}. (*a*) Perfect resolution. (*b*) Including finite pulse-height resolution of the Cerenkov counter. Broken lines on figure show corresponding energy divisions. Table in fig. 14(*a*) relates the measured energy E_m (in GeV per nucleon) of each energy division to an effective energy of that division, and shows the ratio of the number of nuclei above E to the number of nuclei measured to be above E_m. This ratio is the overlap correction, as defined in the text.

small table in figure 14*a* relates the measured energy of each division to the effective actual energy of that division and gives the overlap correction needed on each integral point, i.e., the ratio of the true number of nuclei above E to the number of nuclei measured to be above E_m. Except for the highest energies E is very close to E_m, N is close to N_m, and no corrections are needed. The highest energy division corresponds to $E_m = \infty$ and is for practical purposes as high as it is advantageous to go. While there exists no fixed upper limit, requiring a still higher E_m will rapidly reduce the sample size $N_m(E_m)$ without a significant increase in the median energy of the sample. The energy corresponding to $E_m = \infty$ (64.4 GeV per nucleon) is then roughly the maximum energy above which one can measure the composition with this counter, and is of the same order as the maximum resolvable energy defined by equation (2) (63.2 GeV per nucleon).

In contrast to unfolding, equation (A1) does not provide an estimate of the error in the overlap correction. We have in this analysis ignored these errors,

since the overlap errors on the different points are highly *anticorrelated* and they do not affect the accuracy of the resulting spectral index. By anticorrelated errors we mean that the errors σ_i in a set of variables x_i have a negative or inverse correlation, such that if $y = y(x_i)$,

$$\sigma_y^2 < \sum \sigma_i^2 (\partial y/\partial x_i)^2 . \quad \text{(A4)}$$

Here σ_y is the resulting error on y.

REFERENCES

Audouze, J., and Cesarsky, C. J. 1973, *Nature Phys. Sci.*, **241**, 98.
Badhwar, G. D., and Osborn, R. W. 1973, 13th International Cosmic-Ray Conference (Denver), Vol. **1**, p. 195.
Balasubrahmanyan, V. K., and Ormes, J. F. 1973, *Ap. J.*, **186**, 109.
Brown, J. W., Stone, E. C., and Vogt, R. E. 1973, 13th International Cosmic-Ray Conference (Denver), Vol. **1**, p. 556.
Cartwright, B. 1973, *Ap. Letters*, **14**, 157.
Cassé, M., Koch, L., Lund, N., Meyer, J. P., Peters, B., Soutoul, A., and Tandon, S. N. 1971, Proceedings of the 12th International Conference on Cosmic Rays (Hobart), Vol. **1**, p. 241.
Cesarsky, C. J., and Audouze, J. 1973*a*, preprint, California Institute of Technology.
———. 1973*b*, 13th International Cosmic-Ray Conference (Denver), Vol. **1**, p. 189.
Cowsik, R., Pal, Y., Tandon, S. N., and Verma, R. P. 1967, *Phys. Rev.*, **158**, 1238.
Cowsik, R., and Wilson, L. W. 1973, 13th International Cosmic-Ray Conference (Denver), Vol. **1**, p. 500.
Júliusson, E. 1973, 13th International Cosmic-Ray Conference (Denver), Vol. **1**, p. 178.
Júliusson, E., and Meyer, P. 1973, *Ap. Letters*, **14**, 153.
Júliusson, E., Meyer, P., and Müller, D. 1972, *Phys. Rev. Letters*, **29**, 445.
———. 1973, 13th International Cosmic-Ray Conference (Denver), Vol. **1**, p. 373.
Katcoff, S., Kaufman, S. B., Steinberg, E. P., Weisfield, M. W., and Wilkins, B. D. 1973, *Phys. Rev. Letters*, **30**, 1221.
Kegel, W. H. 1973, *Astr. and Ap.*, **26**, 287.
Mason, G. M. 1972, *Ap. J.*, **171**, 139.
Meneguzzi, M. 1973*a*, 13th International Cosmic-Ray Conference (Denver), Vol. **1**, p. 378.
———. 1973*b*, *Nature Phys. Sci.*, **241**, 100.
Ormes, J. F., and Balasubrahmanyan, V. K. 1973, *Nature Phys. Sci.*, **241**, 95.
Ormes, J. F., Balasubrahmanyan, V. K., and Arens, J. F. 1973, 13th International Cosmic-Ray Conference (Denver), Vol. **1**, p. 157.
Ramaty, R., Balasubrahmanyan, V. K., and Ormes, J. F. 1973, *Science*, **180**, 731.
Rengarajan, T. N., Stephens, S. A., and Verma, R. P. 1973, 13th International Cosmic-Ray Conference (Denver), Vol. **1**, p. 384.
Shapiro, M. M., and Silberberg, R. 1970, *Ann. Rev. Nuc. Sci.*, **20**, 323.
Silverberg, R. F., and Ramaty, R. 1973, *Nature Phys. Sci.*, **243**, 134.
Smith, L. H., Buffington, A., Smoot, G. F., Alvarez, L. W., and Wahlig, M. A. 1973, *Ap. J.*, **180**, 987.
Webber, W. R. 1974, 13th International Cosmic-Ray Conference (Denver), Vol. 5, p. 3568.
Webber, W. R., Damle, S. V., and Kish, J. C. 1972, *Ap. and Space Sci.*, **15**, 245.
Webber, W. R., Lezniak, J. A., and Kish, J. C. 1973*a*, 13th International Cosmic-Ray Conference (Denver), Vol. **1**, p. 248.
Webber, W. R., Lezniak, J. A., Kish, J. C., and Damle, S. V. 1973*b*, *Nature Phys. Sci.*, **241**, 96.

EINAR JÚLIUSSON
Enrico Fermi Institute and Department of Physics, Laboratory for Astrophysics and Space Research, University of Chicago